


# Engineering Functional Vascularized Beige Adipose Tissue from Microvascular Fragments of Models of Healthy and Type II Diabetes Conditions

Journal of Tissue Engineering  
Volume 13: 1–17  
© The Author(s) 2022  
Article reuse guidelines:  
sagepub.com/journals-permissions  
DOI: 10.1177/20417314221109337  
journals.sagepub.com/home/tej



Francisca M. Acosta<sup>1,2,3†</sup>, Katerina Stojkova<sup>1†</sup>, Jingruo Zhang<sup>3</sup>,  
Eric Ivan Garcia Huitron<sup>1</sup>, Jean X. Jiang<sup>3</sup>,  
Christopher R. Rathbone<sup>1,2</sup> and Eric M. Brey<sup>1,2</sup> 

## Abstract

Engineered beige adipose tissues could be used for screening therapeutic strategies or as a direct treatment for obesity and metabolic disease. Microvascular fragments are vessel structures that can be directly isolated from adipose tissue and may contain cells capable of differentiation into thermogenic, or beige, adipocytes. In this study, culture conditions were investigated to engineer three-dimensional, vascularized functional beige adipose tissue using microvascular fragments isolated from both healthy animals and a model of type II diabetes (T2D). Vascularized beige adipose tissues were engineered and exhibited increased expression of beige adipose markers, enhanced function, and improved cellular respiration. While microvascular fragments isolated from both lean and diabetic models were able to generate functional tissues, differences were observed in regard to vessel assembly and tissue function. This study introduces an approach that could be employed to engineer vascularized beige adipose tissues from a single, potentially autologous source of cells.

## Keywords

Beige adipose tissue, fat, microvascular fragments, tissue engineering, type 2 diabetes

Date received: 10 January 2022; accepted: 8 June 2022

## Introduction

Obesity is a leading cause of mortality worldwide. Over 42% of adults in the United States alone are obese,<sup>1</sup> contributing to increases in Type II Diabetes Mellitus (T2D), cardiovascular disease,<sup>2</sup> certain cancers,<sup>3</sup> and hypertension.<sup>4</sup> In addition to serious health consequences, obesity presents an enormous financial burden on the healthcare system, with costs of over \$149 billion annually in the United States.<sup>5</sup> New therapies for the treatment of obesity would have a dramatic impact on healthcare and society.

Adipose tissue is essential for maintaining energy balance and a critical regulator of systemic metabolic function.<sup>6</sup> Excess energy in obese individuals leads to the expansion of white adipose tissue (WAT), a storage depot

that also plays a role in the complex signaling processes regulating metabolic health.<sup>7</sup> While the majority of

<sup>1</sup>Department of Biomedical Engineering and Chemical Engineering, University of Texas at San Antonio, San Antonio, TX, USA

<sup>2</sup>UTSA-UTHSCSA Joint Graduate Program in Biomedical Engineering, San Antonio, TX, USA

<sup>3</sup>Department of Biochemistry and Structural Biology, University of Texas Health Science Center, San Antonio, TX, USA

<sup>†</sup>These authors contributed equally to this work

### Corresponding author:

Eric M. Brey, Department of Biomedical Engineering and Chemical Engineering, University of Texas at San Antonio, One UTSA Circle, San Antonio, TX 78249, USA.  
Email: eric.brey@utsa.edu



adipose tissue is WAT, brown adipose tissue (BAT) is a distinct depot that can exhibit an increased capacity for energy expenditure and heat generation.<sup>8</sup> Activation of BAT is under investigation as a therapeutic target for combating the adverse metabolic consequences associated with obesity and its comorbidities; however, the small volume of BAT in adults could limit the ability to have a significant and sustained impact on systemic metabolism.<sup>9–14</sup>

A subpopulation of cells present in subcutaneous WAT depots can be induced to function as energy-burning cells.<sup>15,16</sup> These “beige” or “brite” cells exhibit morphological characteristics similar to brown fat, including the presence of multilocular lipid droplets, increased mitochondria, and increased metabolic activity as characterized by the process of mitochondrial uncoupling.<sup>16</sup> An important molecular signature of beige and brown adipocytes is the expression of uncoupling protein 1 (UCP1). Upon activation by fatty acids, UCP1 uncouples oxidative phosphorylation in mitochondria from the production of ATP, disrupting ATP synthesis and dissipating energy as heat (thermogenesis), a cycle also referred to as mitochondrial proton leak.<sup>9</sup> These features culminate in intense catabolic activity collecting glucose, lipids, and oxygen from the blood at a higher rate, aiding in glucose clearance and reducing the demand for insulin secretion. In animal models, an increase in beige adipocytes has beneficial effects on whole-body metabolism, body weight, and glucose and lipid homeostasis.<sup>12,17</sup> Due to these potential benefits, the “browning” of subcutaneous WAT may be a means to treat and/or prevent obesity, T2D, and other metabolic disorders.<sup>12,18–20</sup>

Three-dimensional engineered *in vitro* models of functional beige adipose tissues can be used to study metabolic conditions, identify therapeutic targets, and evaluate treatment options.<sup>21,22</sup> However, the majority of adipose models emphasize WAT,<sup>23–25</sup> with 3D engineered beige adipose tissue in relatively early stages of development.<sup>9,21–23,26–28</sup> However, the functional and structural relevance of these models to beige adipose tissue is limited. Specifically, current models fail to recreate the structural and functional complexity of beige adipose tissue, such as increased mitochondrial biogenesis, and most importantly, the incorporation of a vascular network, which would enable rapid vascularization post transplantation and recreation of intrinsic beige adipose tissue composition.

Beige and white adipocyte precursors reside in a distinct perivascular niche in adipose tissues.<sup>29</sup> This close proximity to vasculature is critical for WAT expansion and the development of functional beige adipose tissues.<sup>30</sup> This relationship may be particularly important in disease states where the function of the vasculature or precursor cells may be altered. Models that recreate this close relationship between vessels and adipose precursors could be used to gain new insight into beige adipose tissue development and function. Microvascular fragments (MVF) are

microvessel segments (arterioles, venules, and capillaries) isolated from adipose tissue and contain cells/structures essential for vascularization without the need for extensive *in vitro* manipulation. Importantly, MVF also contain perivascular stem cells with multi-differentiation potential, including adipogenic differentiation.<sup>31,32</sup> Collectively, MVF are a unique tool to exploit the relationship between vascularization and adipogenesis and provide an autologous source of both vessels and adipocytes. In this work, vascularized beige and white adipose tissue models were developed with MVF derived from both healthy and T2D animals. The structure and function of the tissue models were analyzed to support the contention that this systematic investigation produced a valuable microtissue model that may be used to understand or develop treatments for obesity and metabolic disease.

## Results

### *Expression of white and beige adipogenic markers by MVF isolated from lean and diabetic rats*

Microvascular fragments (MVF) were isolated from subcutaneous adipose tissues from lean (L-MVF) and diabetic (Db-MVF) rats, suspended in fibrin gels, and grown for 14 days in growth media (GM), white adipogenic media (WAM), or beige adipogenic media (BAM) conditions (Figure 1(a)). L-MVF and Db-MVF exhibited an interconnected network of lectin-positive cells when cultured in GM (Figure 1(b)). Qualitatively, the highest degree of network formation was observed in the lean GM group (Figure 1(b)). Quantitative analyses were performed on three-dimensional confocal images of the fibrin scaffolds to compare vessel network formation. Vessel density in L-MVF cultured in GM was higher than all other groups, including Db-MVF grown in GM ( $1.1 \pm 0.08$  vs.  $0.75 \pm 0.06\%$ ,  $p < 0.0001$ ) (Figure 1(c)).

When exposed to WAM or BAM differentiation media, lipid loading was confirmed by BODIPY staining with MVF from both lean and diabetic animals (Figure 1(b)). Qualitatively, lipid levels appeared greater in Db-MVF and appeared to be higher with exposure to BAM relative to WAM (Figure 1(b)). Quantitative analyses were performed on three-dimensional confocal images of the fibrin scaffolds to compare across experimental groups. The MVF grown in GM exhibited negligible lipid formation in either lean or diabetic animals ( $0.002 \pm 0.0006$  and  $0.001 \pm 0.0003\%$ , respectively). On the other hand, there was a significantly greater level of BODIPY staining with WAM or BAM compared to GM. L-MVF and Db-MVF treated with WAM had similar levels of lipid droplet formation ( $0.33 \pm 0.03$  and  $0.32 \pm 0.03\%$ , respectively), and were not different from L-MVF treated with BAM ( $0.34 \pm 0.03\%$ ). Interestingly, Db-MVF treated with BAM

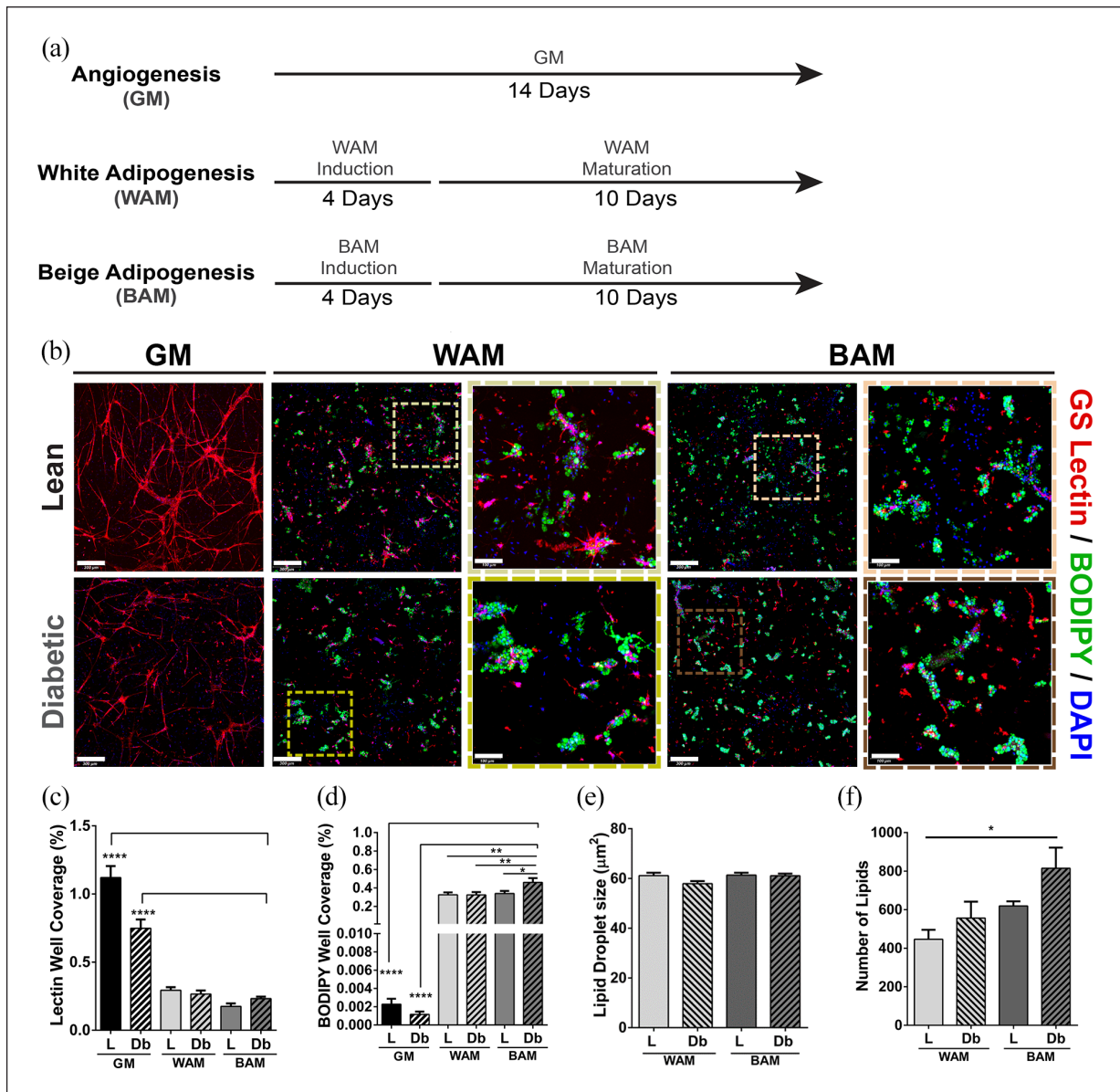


**Figure 1.** Immunofluorescence analysis of direct lean (L) and diabetic (Db) microvascular fragment beige adipogenic differentiation after 14 days. (a) Schematic describing the first experiment and showing the different groups tested. (b) Representative confocal images of microvascular fragments grown in fibrin scaffolds and stained with GS-Lectin I (red) to visualize vascular network formation and BODIPY (green) to identify the presence of lipid droplets (full view scale bar = 300 µm, inset scale bar = 100 µm). (c and d) Quantitative analysis of vessel and lipid formation as determined with GS-Lectin I (Lectin) or boron-dipyrromethene (BODIPY) accumulation, respectively. Quantification performed as a measurement of % well coverage within wells. (e and f) Quantification of lipid droplet size and number of lipids, respectively, per well. Subcutaneous (SUBQ) fat was used as the source of microvascular fragments. Results are reported as mean  $\pm$  standard error of two experimental replicates ( $n=6$  per experiment). \* $p < 0.05$ , \*\* $p < 0.01$ , \*\*\* $p < 0.001$ , \*\*\*\* $p < 0.0001$ . Lines across the experimental group indicate statistical significance relative to all groups.

exhibited significantly greater lipid loading than any other condition (Db BAM vs. L WAM:  $0.46 \pm 0.05$  vs  $0.33 \pm 0.03$ ,  $p=0.007$ , vs. Db WAM  $0.32 \pm 0.03$ ,  $p=0.006$ , and vs. L BAM  $0.34 \pm 0.03\%$ ,  $p=0.01$ ; Figure 1(d)). In addition, the size and number of the lipid droplets formed in each group was analyzed (Figure 1(e) and (f)). There were no differences in the lipid droplet size between all

experimental groups, but there was a significant difference in the number of lipid droplets between L-MVF treated with WAM and Db-MVF treated with BAM ( $447 \pm 49$  vs.  $815 \pm 107$ ,  $p=0.01$ ), consistent with an overall increase in lipid area (Figure 1(d)).

Expression of adipogenic and thermogenic markers were examined by RT-qPCR (Comparison of D1 values

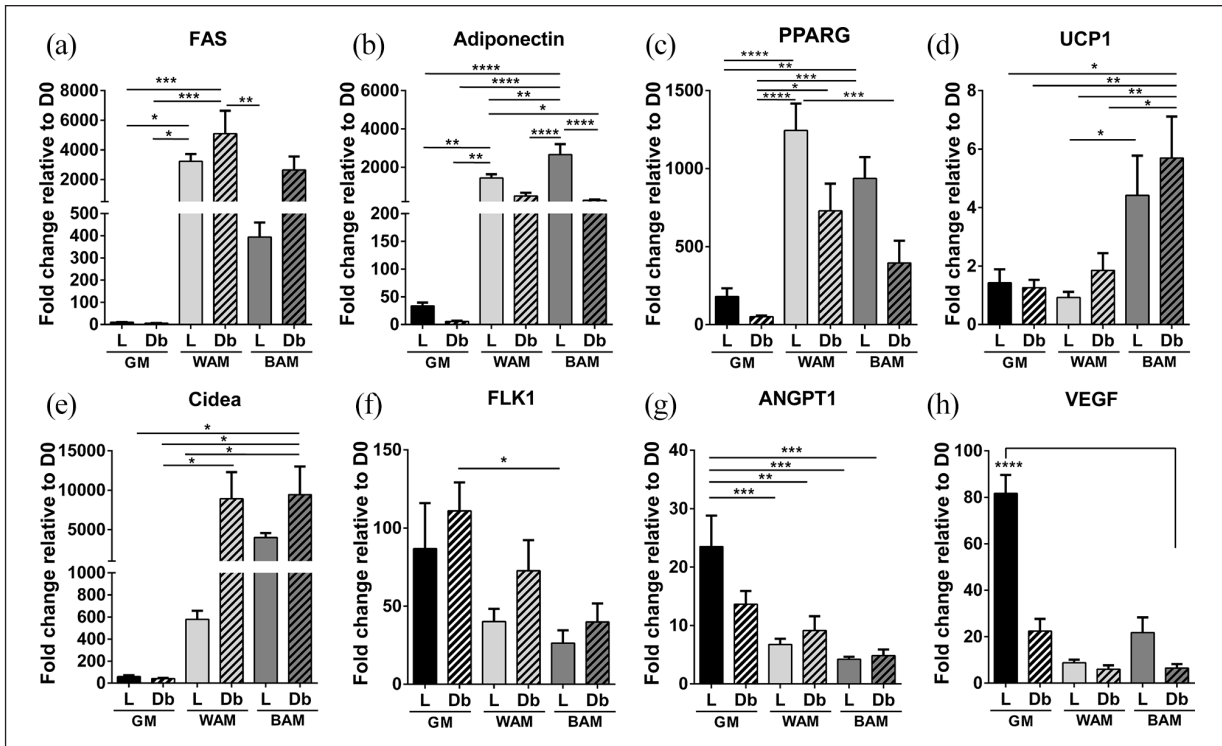


**Figure 2.** RT-qPCR analysis of main adipogenic, thermogenic, and angiogenic genes of microvascular fragments extracted from SUBQ fat of lean (L) and diabetic (Db) rats after 14 days in culture. (a–c) Fold expression of several adipogenic genes, Fatty acid synthase (FAS), Adiponectin, and peroxisome proliferator-activated receptor gamma (PPARG). (d and e) Fold expression of several thermogenic genes, uncoupling protein 1 (UCP1) and cell death-inducing DNA fragmentation factor alpha-like effector A (Cidea). (f–h) Fold expression of several angiogenic genes, Fetal liver kinase 1 (FLK1), Angiotensin-converting enzyme 1 (ACE1), and vascular endothelial growth factor (VEGF). Results are reported as mean  $\pm$  standard error of two experimental replicates ( $n=4$  per experiment). \* $p < 0.05$ , \*\* $p < 0.01$ , \*\*\* $p < 0.001$ , \*\*\*\* $p < 0.0001$ .

between L-MVF and Db-MVF are shown in Supplemental Figure S2). Genes associated with adipogenesis, including adiponectin, fatty acid synthase (FAS), and peroxisome proliferator-activated receptor gamma (PPARG), were greater in WAM and BAM conditions in comparison to controls (GM, Figure 2(a)–(c)). FAS, an enzyme that catalyzes the formation of long-chain fatty acids in adipose tissue, was expressed in MVF from both lean and diabetic animals cultured under WAM and BAM conditions with the highest expression levels in the Db-MVF group grown in WAM (Figure 2(a)). Adiponectin, a protein expressed primarily in mature adipocytes, was also expressed in L-MVF and Db-MVF exposed to WAM and BAM conditions. Adiponectin expression levels were greater in L-MVF cultured in both WAM and BAM conditions. Additionally, L-MVF cultured in BAM conditions had significantly higher expression levels in comparison to all experimental groups ( $p < 0.0001$ , Figure 2(b)). PPARG, a protein that regulates adipocyte differentiation, exhibited similar trends with significantly greater expression levels in L-MVF cultured in WAM and BAM compared to GM groups ( $p < 0.0001$  and  $p < 0.001$ , respectively). There were no significant differences in PPARG

expression levels between L-MVF and Db-MVF. However, expression levels demonstrated a trend toward lower levels in Db-MVF (Figure 2(c)).

Uncoupling protein 1 and cell death-inducing DNA fragmentation factor alpha-like effector A (UCP1 and Cidea, respectively) are genes involved in thermogenesis that are upregulated in brown and beige adipose tissues.<sup>8</sup> The expression of UCP1, a mitochondrial protein involved in thermogenic respiration, was higher in both L-MVF and Db-MVF exposed to BAM relative to GM and WAM groups, reaching statistical significance in L-MVF cultured in BAM relative to WAM ( $p=0.036$ ). Interestingly, expression of UCP1 was highest in the Db-MVF BAM group (~sixfold), with levels significantly higher than L-MVF and Db-MVF WAM and GM groups. There was no significant difference in UCP1 levels between L-MVF and Db-MVF exposed to BAM conditions (Figure 2(d)). Cidea, a regulator of the thermogenic function in brown/beige fat,<sup>33</sup> was increased in Db-MVF treated with both WAM and BAM. Db-MVF exhibited significantly higher expression of Cidea in comparison to all GM groups and L-MVF treated with WAM (Figure 2(e)). These results indicate that L-MVF and Db-MVF contain cells that can

be induced to express markers of beige or brown adipose tissue. In addition, Db-MVF exhibited increased expression of thermogenic markers relative to lean animals.

In addition to genes associated with adipogenesis, genes involved in angiogenesis were evaluated. Levels of fetal liver kinase 1 (FLK1), an early angiogenic marker, was higher in all experimental groups relative to day 0. FLK1 was slightly greater in Db-MVF cultured in GM, WAM, and BAM conditions relative to L-MVF, but the differences were not statistically significant (Figure 2(f)). Angiopoietin-1 (ANGPT1), a late angiogenic marker, exhibited the highest expression in L-MVF exposed to GM, with statistical significance relative to all WAM and BAM culture conditions ( $p < 0.005$ , Figure 2(g)). Expression of vascular endothelial growth factor (VEGF), a key promoter of angiogenesis, was increased in all experimental groups relative to day 0 with the L-MVF GM group (~81-fold increase) significantly higher than all other conditions ( $p < 0.0001$ , Figure 2(h)). Collectively, these results suggest that Db-MVF may exhibit a decreased capacity for angiogenesis.

### Functional assessment of engineered adipose tissues

Function of the engineered tissues was first evaluated based on tissue glucose uptake under basal conditions and following insulin stimulation (Figure 3(a)). Insulin-stimulated glucose uptake (ISGU) was significantly higher in L-MVF or Db-MVF treated with BAM, as well as Db-MVF treated with WAM, relative to L-MVF in WAM conditions ( $p = 0.0004$ ,  $p = 0.005$ , and  $p = 0.0005$ , respectively). Lipolysis was used as an additional measure of adipose tissue function. Mature adipocytes in culture respond to cAMP analogs, such as isoproterenol, that stimulate lipolysis, which can be measured by the level of glycerol released in the culture media (Figure 3(b)). There was no difference in glycerol levels between control and isoproterenol stimulated L-MVF and Db-MVF grown in GM. On the other hand, Db-MVF cultured in WAM conditions and L-MVF and Db-MVF cultured in BAM conditions exhibit an increased release of glycerol relative to the controls following stimulation with isoproterenol. Further, there was a significant increase in lipolytic activity in both L-MVF and Db-MVF in BAM conditions relative to their respective controls ( $6.8 \pm 0.5$  vs.  $4.6 \pm 0.7$ ,  $p = 0.02$  and  $5.6 \pm 0.7$  vs.  $3.3 \pm 0.9$  mmol/well,  $p = 0.01$ ). Finally, both L-MVF and Db-MVF in BAM had a significantly greater level of glycerol compared to all WAM conditions when induced with isoproterenol ( $p < 0.0001$  and  $p < 0.05$ , respectively).

The unique metabolic profile of brown/beige adipose tissue is critical for its potential as a therapeutic approach to the treatment of diabetes and obesity. Therefore, oxygen consumption rate (OCR) measurements were used to

further examine mitochondrial function in culture. OCR was measured while applying oligomycin (inhibiting ATP synthase), FCCP (stimulating maximal respiration), and rotenone/antimycin A (inhibiting the electron transport chain enabling the calculation of nonmitochondrial respiration) in sequence over the course of 3 hours (Figure 3(c)). L-MVF and Db-MVF exposed to WAM and BAM conditions exhibited a significant increase in basal respiration rate relative to L-MVF ( $38.9 \pm 1.8$  vs.  $55.7 \pm 4.4$ ,  $p = 0.0008$ , vs.  $50.2 \pm 2.5$ ,  $p = 0.05$ , vs.  $52.6 \pm 3.2$ ,  $p = 0.02$ , vs.  $53.5 \pm 1.9$  pmol/min,  $p = 0.005$ ) and Db-MVF ( $36.6 \pm 1.9$  pmol/min,  $p = 0.001$ ,  $p = 0.01$ ,  $p = 0.003$ ,  $p = 0.0007$ , respectively) GM groups. However, there was no difference in the basal respiration rate between the L-MVF and Db-MVF exposed to WAM or BAM conditions (Figure 3(d)). Proton leak, a measure of uncoupled respiration, was highest in L-MVF exposed to BAM ( $25.7 \pm 1.3$  pmol/min, Figure 3(e)) with a significant difference relative to L-MVF and Db-MVF grown in GM ( $13.9 \pm 0.5$  and  $14.2 \pm 0.6$  pmol/min,  $p < 0.0001$ ) or WAM ( $22.5 \pm 0.5$ ,  $p = 0.03$  and  $20.3 \pm 0.7$  pmol/min,  $p < 0.0001$ ). No differences were observed between L-MVF and Db-MVF in BAM conditions. Maximum respiration was highest in L-MVF and Db-MVF in BAM ( $33.5 \pm 1.9$  and  $40.8 \pm 2.3$  pmol/min), which was significantly greater than WAM ( $26.7 \pm 0.7$  and  $26.9 \pm 0.9$  pmol/min  $p < 0.05$  and  $p < 0.0001$ , respectively) and GM (L-MVF,  $21.7 \pm 1.3$  and Db-MVF,  $19.1 \pm 0.7$  pmol/min,  $p < 0.0001$ , Figure 3(f)). Interestingly, maximum respiration of Db-MVF was significantly higher than L-MVF grown in BAM conditions ( $p = 0.006$ ). The spare capacity, a measure of the ability of cells to achieve maximum respiration, was also higher in both L-MVF and Db-MVF in BAM with a significantly higher percent in Db-MVF in BAM ( $77 \pm 5\%$ ) relative to GM and WAM ( $p < 0.0001$  Figure 3(g)). These findings correlate with the increased mRNA expression of UCP1 in the Db-MVF scaffolds in BAM conditions (Figure 2(d)).

### Formation of vascularized adipose tissue

Vascularization is critical to the development of adipose tissue.<sup>34–36</sup> It is well-established that MVF can be stimulated to assemble into microvascular networks.<sup>37</sup> However, the extent to which precursor cells retain their adipogenic differentiation capacity following network formation, and whether diabetes affects this capacity, has not been fully resolved. L-MVF and Db-MVF were cultured in GM for 7 days prior to exposure to either white or beige adipogenic media for 14 days (GM-WAM or GM-BAM). Control scaffolds consisted of MVF cultured in GM for 21 days (GM-GM) (Figure 4(a)). The tissue constructs were first stained for lectin and imaged with confocal microscopy to examine structure at 21 days. Qualitatively, MVF derived from both lean and diabetic animals grown for 21 days in control conditions (GM-GM) demonstrated extensive vessel

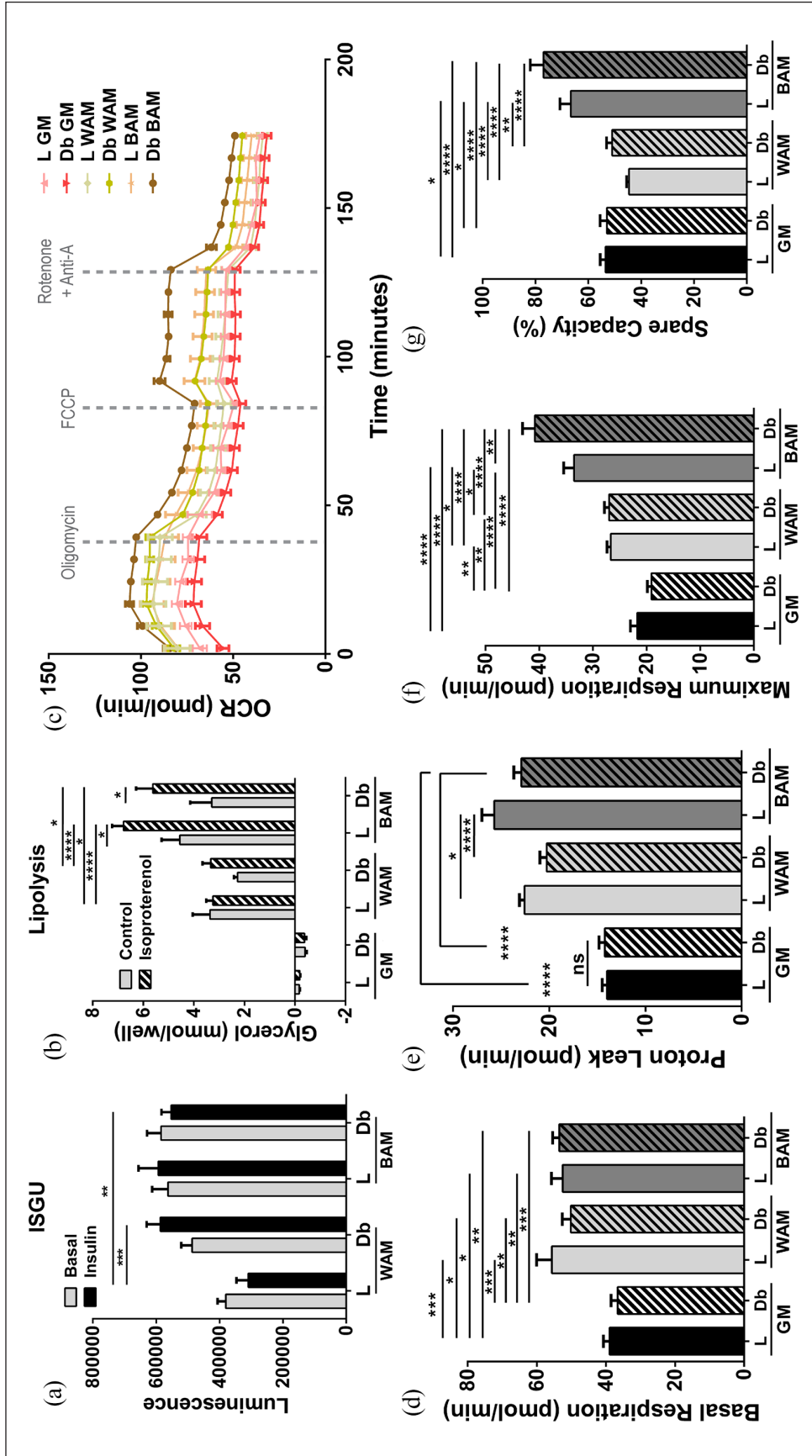


**Figure 3.** Functional analysis of beige adipose tissue formation in direct adipogenic culture of lean and diabetic microvascular fragments. Microvascular fragments (MVFs) from subcutaneous fat of lean (L) and diabetic (Db) rats were directly exposed to white (WAM) or beige (BAM) adipogenic media for 14 days. At the end of the 14 days (a) Insulin stimulated glucose uptake (ISGU)  $\pm$  insulin, to stimulate glucose uptake and (b) lipolysis  $\pm$  isoproterenol, to stimulate lipolysis, was measured. (c-g) Oxygen Consumption Rate (OCR) trace was determined using a Seahorse XF96 Analyzer among the different groups, basal respiration, proton leak, maximal respiration, and spare capacity were calculated. Results are reported as mean  $\pm$  standard error of two experimental replicates ( $n = 4$  per experiment). \* $p < 0.05$ , \*\* $p < 0.01$ , \*\*\* $p < 0.001$ , \*\*\*\* $p < 0.0001$ , \*\*\*\*\* $p < 0.00001$ .

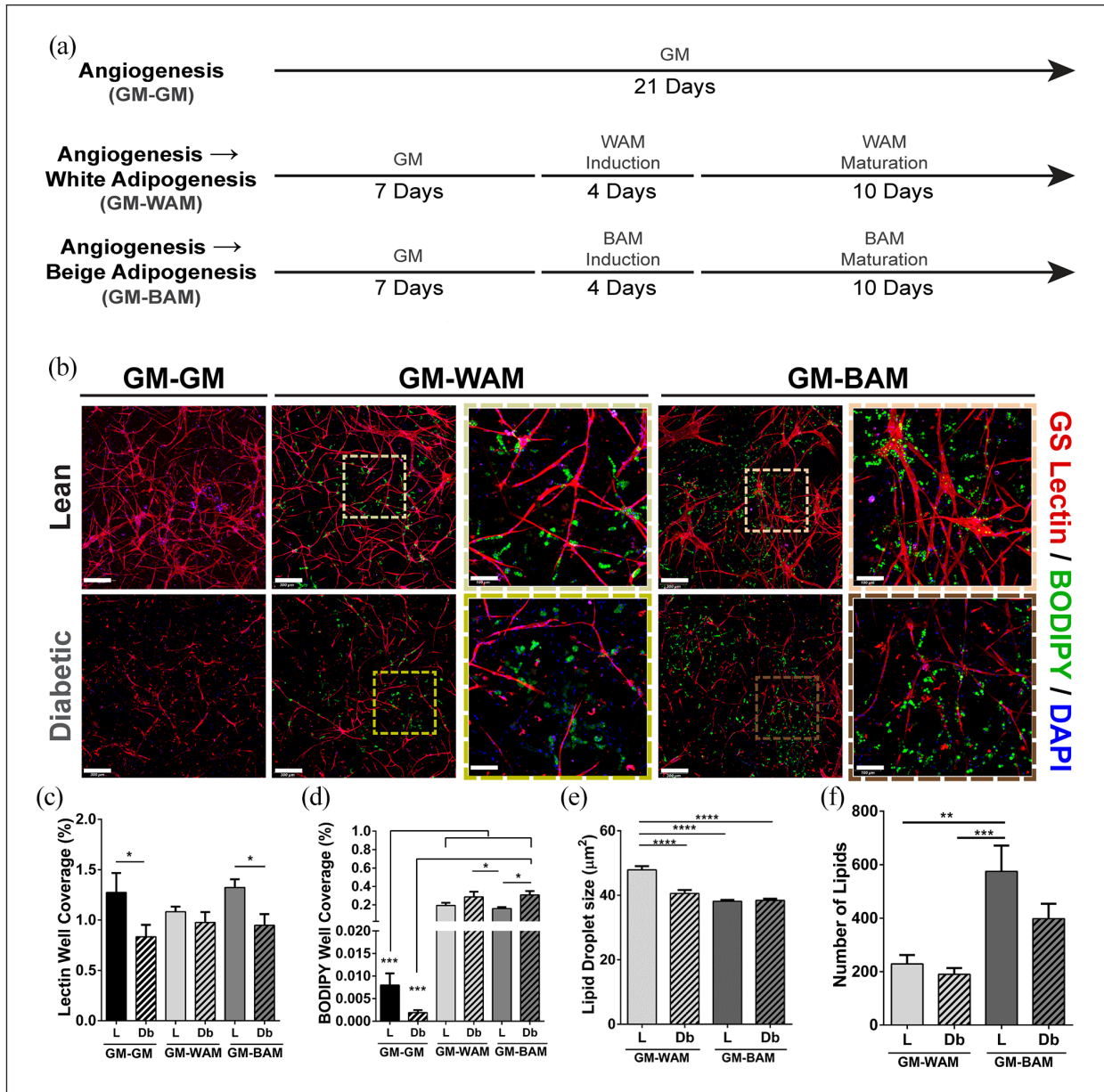


**Figure 4.** Immunofluorescence analysis of indirect lean (L) and diabetic (Db) microvascular fragment beige adipogenic differentiation after 21 days. (a) Schematic describing the second experiment and showing the different groups tested. (b) Representative confocal images of microvascular fragments grown in fibrin scaffolds and stained with GS-Lectin I (red) to visualize vascular network formation and BODIPY (green) to identify the presence of lipid droplets (full view scale bar = 300 μm, inset scale bar = 100 μm). (c and d) Quantitative analysis of vessel and lipid formation as determined with GS Lectin I (Lectin) or boron-dipyrromethene (BODIPY) accumulation, respectively. Quantification performed as a measurement of % well coverage within wells. (e and f) Quantification of lipid droplet size and number of lipids, respectively per well. Subcutaneous (SUBQ) fat was used as the source of microvascular fragments. Results are reported as mean ± standard error of two experimental replicates ( $n=6$  per experiment). \* $p < 0.05$ , \*\* $p < 0.01$ , \*\*\* $p < 0.001$ , \*\*\*\* $p < 0.0001$ . Lines across the experimental group indicate statistical significance relative to all groups.

network formation (Figure 4(b)). However, the vessel structures appeared smaller with less connections in the Db-MVF. The L-MVF cultured in growth media for 7 days prior to 14 days of differentiation (GM-WAM and GM-BAM) exhibited branched vascular network formation

together with clustered lipid droplets throughout the scaffold (Figure 4(b)). On the other hand, the Db-MVF cultured in the same conditions exhibited reduced vessel formation, particularly in the GM-BAM group (Figure 4(b)). Quantitatively, the degree of network formation

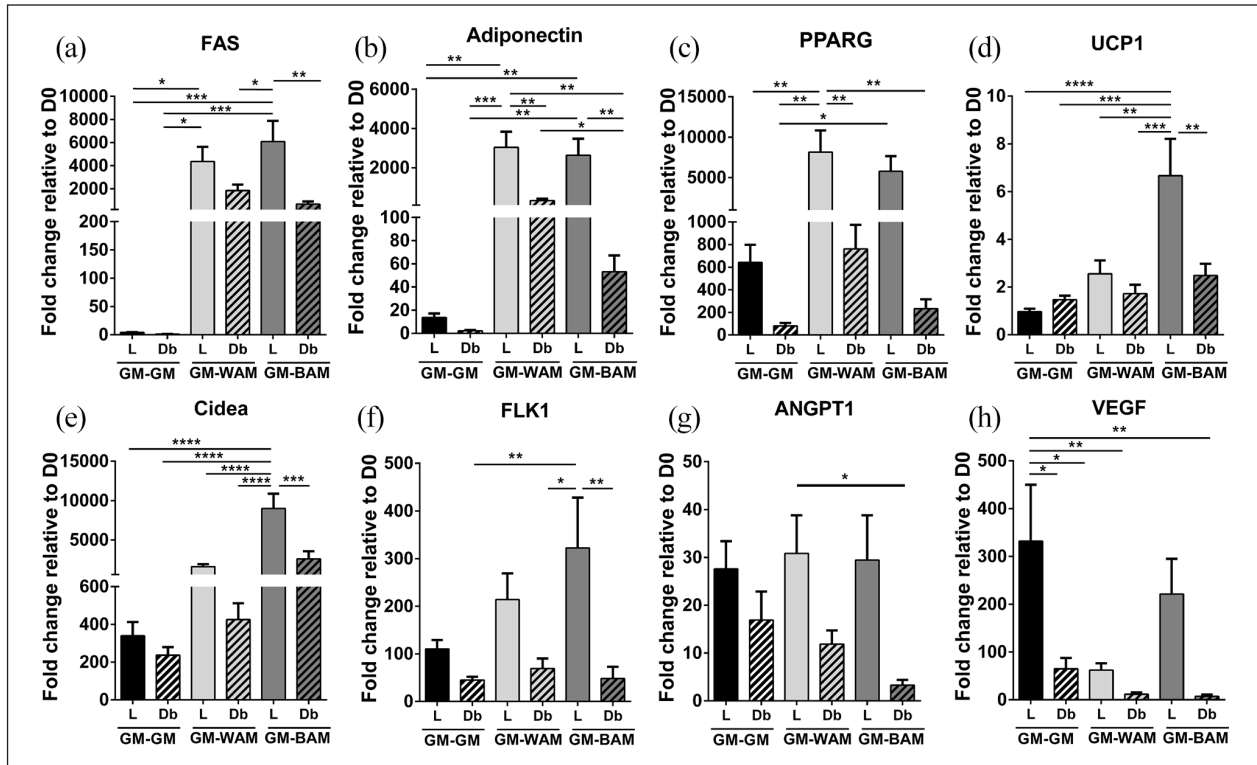


**Figure 5.** RT-qPCR analysis of main adipogenic, thermogenic, and angiogenic genes of microvascular fragments extracted from SUBQ fat of lean (L) and diabetic (Db) rats after 21 days in culture. (a–c) Fold expression of several adipogenic genes, Fatty acid synthase (FAS), Adiponectin, and peroxisome proliferator-activated receptor gamma (PPARG). (d and e) Fold expression of several thermogenic genes, uncoupling protein I (UCPI) and cell death-inducing DNA fragmentation factor alpha-like effector A (Cidea). (f–h) Fold expression of several angiogenic genes, Fetal liver kinase I (FLK1), Angiopoietin-I (ANGPT1), and vascular endothelial growth factor (VEGF). Results are reported as mean  $\pm$  standard error of two experimental replicates ( $n=4$  per experiment). \* $p < 0.05$ , \*\* $p < 0.01$ , \*\*\* $p < 0.001$ , \*\*\*\* $p < 0.0001$ .

was at similar levels for the L-MVF cultured under all three culture conditions ( $1.3 \pm 0.2$ ,  $1.1 \pm 0.05$ , and  $1.3 \pm 0.08\%$ , respectively). Similarly, the percent of lectin staining in Db-MVF did not exhibit differences with culture conditions ( $0.83 \pm 0.1$ ,  $0.97 \pm 0.1$ , and  $0.95 \pm 0.1\%$ , respectively). However, the vascular network formation in L-MVF was generally higher than in Db-MVF. The lean control and GM-BAM groups exhibit a significantly higher percent of angiogenesis in respect to the Db-MVF ( $p=0.03$  and  $p=0.05$ , respectively, Figure 4(c)).

Lipid formation appeared higher in L-MVF and Db-MVF in GM-WAM and GM-BAM relative to GM-GM. Clusters of lipid droplets were present in close proximity to vessels. Quantitatively, BODIPY staining from L-MVF and Db-MVF grown in GM-WAM and GM-BAM was significantly greater than control groups (GM-GM). In general, Db-MVF had greater BODIPY staining in both GM-WAM and GM-BAM conditions relative to L-MVF. There was a statistically significant difference between the Db-MVF treated with GM-BAM and L-MVF treated with GM-BAM ( $0.3 \pm 0.04$  vs.  $0.1 \pm 0.01\%$ ,  $p=0.01$ , Figure 4(d)). The size of lipid droplets of MVF from both L-MVF and Db-MVF in the

GM-BAM conditions were significantly smaller than L-MVF in GM-WAM ( $38.2 \pm 0.4$ ,  $38.4 \pm 0.5$  vs.  $47.9 \pm 0.4 \mu\text{m}^2$ ,  $p < 0.0001$ , Figure 4(e)). There was a significantly greater number of lipid droplets in L-MVF in GM-BAM compared to L-MVF and Db-MVF in GM-WAM ( $575 \pm 96$  vs.  $229 \pm 33$ ,  $p=0.002$  and vs.  $190 \pm 23$ ,  $p=0.0005$ , Figure 4(f)).

Gene expression was analyzed as described above. FAS, adiponectin, and PPARG all showed similar trends of higher expression levels in L-MVF compared to Db-MVF (Figure 5(a)–(c)). Both thermogenic markers, UCP1 and Cidea, showed their highest expression in the L-MVF exposed to GM-BAM. UCP1 expression levels in L-MVF grown in GM-BAM conditions was statistically higher than all other experimental groups (Figure 5(d)). Similarly, L-MVF in GM-BAM conditions had statistically significant higher levels of Cidea expression compared to all other groups. Cidea expression levels were increased by  $\sim 6$  fold in L-MVF GM-BAM relative to GM-WAM (Figure 5(e)). These findings confirm that both L-MVF and Db-MVF retain their ability to express beige adipose markers following a week of pre-vascularization. Overall, L-MVF exposed to both GM-WAM and GM-BAM



conditions exhibited higher expression of genes associated with adipogenesis and thermogenesis than Db-MVF.

Similar to results with direct adipogenic differentiation, the angiogenic genes FLK1, ANGPT1, and VEGF were expressed at higher levels in vascularized tissues using L-MVF relative to Db-MVF under all three differentiation conditions (Figure 5(f)–(h)). FLK1 expression in the L-MVF GM-BAM group (~322 fold) was significantly higher than Db-MVF (~48-fold,  $p=0.007$ , Figure 5(f)). ANGPT1 showed similar expression levels in L-MVF across the three growth conditions (~27, ~30, and ~29 fold, respectively) and were higher relative to Db-MVF (Figure 5(g)). The highest VEGF expression was in the L-MVF GM-GM group (~331-fold), which was significantly higher relative to all experimental groups except for L-MVF in GM-BAM conditions (Figure 5(h)). Similar to the other angiogenic markers, the Db-MVF GM-BAM group had the lowest expression levels of VEGF, which agrees with the reduced vessel network formation observed in the immunofluorescence staining (Figure 4(b)).

### Functional assessment of the engineered vascularized adipose tissue

Functional testing was performed on the vascularized adipose scaffolds. All experimental groups exhibited increased glucose uptake with insulin stimulation (Figure 6(a)). In addition, relative glucose uptake in the vascularized tissues exposed to GM-BAM conditions trended higher than those exposed to GM-WAM with both L-MVF and Db-MVF. There was an overall trend of increased lipolysis in GM-BAM groups in both L-MVF and Db-MVF relative to GM-WAM (Figure 6(b)). There was a significant increase in glycerol levels in the L-MVF in GM-BAM conditions following isoproterenol stimulation ( $7.3 \pm 0.5$  vs.  $4.5 \pm 0.5$  mmol/well,  $p < 0.0001$ ). Additionally, vascularized tissues from L-MVF cultured in GM-BAM contained significantly higher glycerol levels relative to GM-WAM from L-MVF and Db-MVF ( $7.3 \pm 0.5$  vs.  $3.4 \pm 0.3$ , and  $3.6 \pm 0.3$  mmol/well, respectively,  $p < 0.0001$ ) when stimulated with isoproterenol. Notably, isoproterenol stimulation resulted in higher glycerol levels in all adipogenic groups except Db-MVF in GM-WAM. Increased UCP1 expression in brown or beige adipocytes is expected to result in reduced production of reactive oxygen species (ROS).<sup>38</sup> ROS levels in vascularized tissues derived from both L-MVF and Db-MVF and exposed to GM-BAM were significantly lower than GM-GM and GM-WAM (Figure 6(c)).

The metabolic activity of the vascularized adipose tissue models was evaluated by quantifying OCR with exposure to oligomycin, FCCP, and rotenone/antimycin A in sequence over the course of 3 hours (Figure 6(d)). Basal respiration and proton leak showed similar trends, with L-MVF exhibiting slightly higher values than Db-MVF under all three conditions, but there were no significant

differences in basal respiration (Figure 6(e) and (f)). Maximum respiration, on the other hand, was higher in L-MVF and Db-MVF in GM-BAM relative to GM-GM and GM-WAM (Figure 6(g)). The maximum respiration was highest in L-MVF in GM-BAM ( $53.5 \pm 2.9$  pmol/well) which was significantly greater than MVF in GM-GM ( $23.4 \pm 2.1$  and  $23.2 \pm 2.1$  pmol/well for L and Db,  $p < 0.0001$ ) and GM-WAM ( $35.5 \pm 1.9$ ,  $p = 0.002$  for L and vs.  $32.4 \pm 2.8$  pmol/well,  $p = 0.0002$  for Db). Finally, both L-MVF and Db-MVF in GM-BAM had a significantly greater percent spare capacity relative to MVF in GM-GM and GM-WAM (Figure 6(h)). These data indicate that L-MVF and Db-MVF in GM-BAM conditions were more metabolically active than the scaffolds exposed to either GM-WAM or GM-GM.

### Discussion

A number of medical and surgical approaches are under investigation that attempt to exploit the enhanced metabolic activity of brown or beige adipose tissues as a treatment for obesity or metabolic disease.<sup>39</sup> However, the limited volume of tissue available, poor understanding of adipose tissue physiology, and potential safety concerns of pharmacological agents limits successful translation of these approaches.<sup>9</sup> Another option being considered is engineering of beige or brown adipose tissues that are subsequently transplanted in an attempt to transform systemic metabolism. Transplanted BAT can decrease body fat, reverse insulin resistance, and improve overall metabolic function in animal models.<sup>9,21,40,41</sup> Engineering adipose tissue constructs with metabolic function and structure similar to BAT using an easily accessible and potential autologous cell source may be a viable therapeutic intervention and could be used as a tool for studying BAT and its metabolic properties.

Microvascular fragments (MVF), isolated from adipose tissue, may provide a straightforward approach for generating vascularized beige adipose tissue.<sup>37,42</sup> MVF can be isolated from autologous adipose tissue depots harvested from adults using standard minimally-invasive procedures.<sup>43</sup> Though MVF-based vascularization has not been carried out in clinical practice, preclinical studies utilizing human MVF isolated from lipoaspirate have been conducted, demonstrating its achievability and potential.<sup>44,45</sup> Previous work from our group and others has demonstrated that in addition to endothelial cell-lined capillaries, MVF are a source of adipose derived stem and progenitor cells, mural cells, and immune cells.<sup>31,32,37</sup> While it is established that MVF can be used to generate white adipose tissue,<sup>31,32,37,46</sup> it was unknown if MVF could be used to generate beige adipose tissue, and to what extent diabetes affects this process.

Exposure of MVF to both white and beige adipogenic media resulted in lipid loading and adipogenic differentiation. When exposed to conditions designed to induce beige

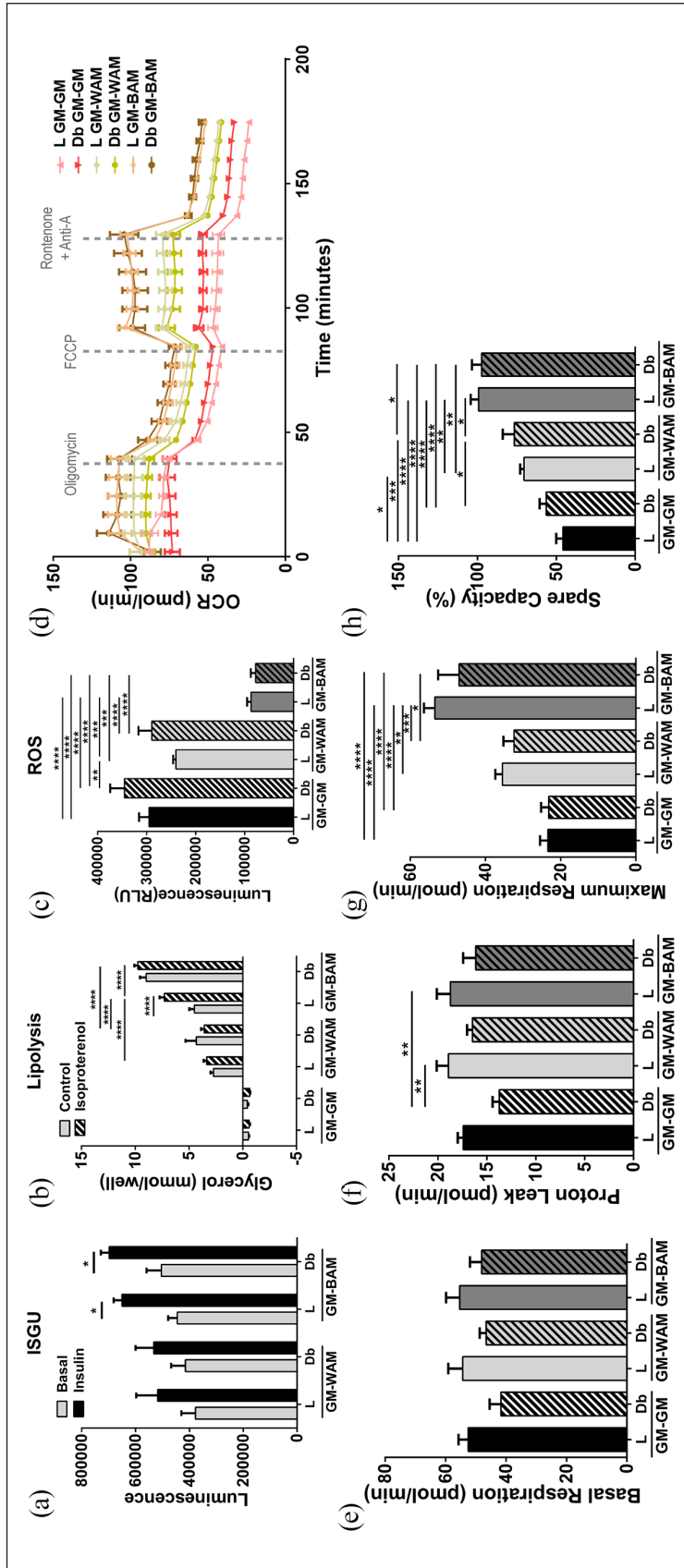


**Figure 6.** Functional analysis of beige adipose tissue formation in indirect adipogenic culture of lean and diabetic microvascular fragments. Microvascular fragments (MVF) from subcutaneous fat of lean (L) and diabetic (Db) rats were indirectly exposed to white (WAM) or beige (BAM) adipogenic media for 21 days. At the end of the 21 days (a) Insulin stimulated glucose uptake (ISGU)  $\pm$  insulin, to stimulate glucose uptake and (b) lipolysis  $\pm$  isoproterenol, to stimulate lipolysis, was measured. (c) Luminescence levels (proportional to  $H_2O_2$  levels) measured by the ROS-GLO assay in the MVF scaffolds exposed to growth media (GM-GM), white (GM-WAM) and beige (GM-BAM) differentiation media. (d–h) Oxygen Consumption Rate (OCR) trace was determined using a Seahorse XF96 Analyzer among the different groups, basal respiration, proton leak, maximal respiration, and spare capacity were calculated. Results are reported as mean  $\pm$  standard error of two experimental replicates ( $n = 4$  per experiment). \* $p < 0.05$ , \*\* $p < 0.01$ , \*\*\* $p < 0.001$ , \*\*\*\* $p < 0.0001$ .

adipocyte differentiation, the MVF increased expression of the thermogenic genes UCP1 and Cidea. The enhanced function of beige adipose tissue over white adipose tissue is critical to its potential for therapeutic impact.<sup>47</sup> The treatment of MVF with beige adipogenic differentiation conditions enhanced their function relative to white adipogenic differentiation conditions and controls. Insulin stimulated glucose uptake was generally higher in the BAM treated groups, which is consistent with characteristics of brown adipose tissue.<sup>48</sup> The beige adipose tissues also exhibited increased lipolysis.<sup>49</sup> Basal levels of lipolysis were increased in all adipogenic media groups; however, only BAM treated groups exhibited an increase in lipolysis with exposure to isoproterenol. For a more detailed analysis of the metabolic function of the tissue, mitochondrial bioenergetics were examined with OCR. Brown and beige adipose tissues are mitochondria rich, a primary reason for their distinguishing “brownish” appearance pathologically. The maximum rate of respiration was significantly higher in BAM treated groups. Proton leak, a measure of basal respiration not coupled to ATP production, also exhibited the highest levels in BAM. Lastly, spare capacity was highest among BAM treated groups, demonstrating that the greatest cell fitness or flexibility in responding to energetic demand was exhibited by beige adipose microtissues. Overall, these results indicate that isolated MVF, from a rodent source, contain cells that can be induced to express markers of beige adipose tissue and, that BAT engineered from MVF from both lean and diabetic models, exhibit key functional characteristics of beige adipose tissue, including improved glucose uptake, lipolysis, and mitochondrial bioenergetics.

Activation of beige adipose tissue is expected to improve systemic metabolism in individuals with obesity and type II diabetes. However, there is limited understanding of the effects of diabetes on the potential formation and function of beige adipose tissues. MVF isolated from an animal model of type II diabetes (Db-MVF) contained cells that could be induced to differentiate and express thermogenic markers at levels similar to MVF from lean animal models (L-MVF). Specifically, among the genes measured, Cidea, plays an important role in triglyceride storage, is found exclusively in BAT in mice, and has a protein expression level that is known to be significantly related to body weight, epididymal adipose tissue mass, and insulin resistance, and there is precedence to believe it might play a role in obesity and development of T2D.<sup>33</sup> Moreover, it has been shown that elevated glucose levels upregulate UCP1 expression, protecting cells from glucose-induced ROS damage.<sup>50</sup> These trends are represented and can be a possible explanation for our results, where we see Cidea having the highest expression level in Db-MVF in both WAM and BAM, and UCP1 being highest in the Db-MVF BAM group. However, it should be noted that the introduction of vascularization (GM-WAM and GM-BAM) removed

aspects of the diabetic phenotype, further demonstrating the importance of introducing vascularization to tissue engineered structures. Functionally, glucose uptake and lipolysis were similar in beige microtissues formed from both L-MVF and Db-MVF. Interestingly, beige microtissues generated from Db-MVF demonstrated the highest mitochondrial activity, significantly higher than L-MVF exposed to BAM. For all other functional outcomes, Db-MVF exhibited similar outcomes to L-MVF. These results suggest that Db-MVF retain beige progenitor cells, and these cells exhibit similar functional outcomes to L-MVF when exposed directly to factors that induce beige adipogenesis.

In the context of diabetes, impaired angiogenesis is a common feature and contributor to diabetes-related morbidities.<sup>51</sup> Investigations in diabetes research, utilizing MVF, have explored using MVF to encourage vascularization of pancreatic islets for type I diabetic (T1D) applications,<sup>52–54</sup> and demonstrated a delayed and reduced angiogenic growth of T1D MVF.<sup>55,56</sup> Though it is reasonable to speculate that the vascularization capacity of type II diabetic MVF might also be altered, as it is in obesity,<sup>36</sup> T1D,<sup>55,56</sup> or aging,<sup>57</sup> that along with work looking into how utilizing a model of type II diabetes as the source of MVF might alter its capacity for tissue engineering applications, had not been previously investigated.

Vascularization is essential for adipose tissue expansion and function.<sup>58,59</sup> Engineering functional beige adipose tissue that survives post-implantation requires an extensive vascular network.<sup>60</sup> Previously, we have shown that coordinating vessel network assembly and adipogenesis requires careful coordination of the timing<sup>32</sup> and composition<sup>9</sup> of the media. Adipose differentiation was examined following an initial 7 day phase of network formation. Vascular network formation was significantly lower with Db-MVF. Expression of genes associated with angiogenesis was also lower in Db-MVF. In the case of obesity, network formation may lag adipose tissue enlargement, leading to lower vascular densities and hypoxia.<sup>34,61</sup> This hypoxic environment is thought to lead to an unbalance and overexpression of pro-angiogenic<sup>62,63</sup> and pro-inflammatory stimuli that can contribute to insulin resistance and diabetes development.<sup>64</sup> Overall, we demonstrate through histological and angiogenic gene expression analysis that Db-MVF have a reduced vascularization capacity. Future work should explore this phenomenon further and investigate tools, such as the co-culture of MVF with supporting cells,<sup>65,66</sup> the preconditioning of MVFs,<sup>43,55,62,63</sup> changes to the seeding density,<sup>67</sup> or modification of the surrounding matrix<sup>68,69</sup> to help improve their performance, from an angiogenic standpoint when coming from a compromised source.

The utilization of MVF as a source of adiposity and vascularization has previously been explored by our group,<sup>32,46</sup> and others.<sup>44</sup> Here we build upon this by

studying vascularized BAT and WAT from L-MVF and Db-MVF. Histological analysis showed successful induction of lipid loading in cells following induction of vessel network formation. While Db-MVF exhibited lower network formation and expression of genes associated with angiogenesis, adipogenic induction with either WAM or BAM following network formation did not disrupt network structure. Instead, MVF serve as an excellent source of network formation that remained stable even when exposed to adipogenic conditions, we contribute this primarily to the careful selection of the adipogenic factors for our studies.<sup>70</sup>

Following 7 days of exposure to growth media known to promote MVF vascular network formation, the 3D culture system retained its capacity for the formation of both white and beige adipocytes. While lipid formation was similar between the groups, expression of adipogenic and thermogenic markers was generally lower in Db-MVF in comparison to L-MVF. Interestingly, vascularized beige fat exhibited an overall improvement in function relative to white fat with little differences between Db-MVF and L-MVF. Insulin sensitivity and lipolysis were enhanced, particularly in groups cultured in BAM. In addition, there was a significant reduction in the production of reactive oxygen species (ROS) in the engineered vascularized beige adipose tissues. ROS levels in obesity, hyperglycemia, or diabetes contribute to cellular death, tissue damage, vascular dysfunction, and ultimately play a pivotal role in diabetic complications.<sup>71,72</sup> In the presence of obesity, WAT mitochondria dysfunctionally contribute to oxidative stress and systemic inflammation leading to insulin resistance contributing to the pathogenesis of T2D.<sup>73,74</sup> Also of note, BAT tissue from obese mice do exhibit increased mitochondrial activity, but this is accompanied by an increase in inflammation and oxidative damage.<sup>75</sup> Although the role of BAT in ROS regulation is not fully established, the decreased levels of ROS in the engineered adipose tissue from Db-MVF suggest that these tissues may reduce ROS production and oxidative damage.<sup>76</sup> The beige vascularized fat also exhibited enhanced cellular respiration, including the highest maximal respiration and spare capacity. Overall, utilizing an indirect approach allowed for the generation of vascularized fat from both L-MVF and Db-MVF. While vascularization and expression of thermogenic genes was lower with Db-MVF, the metabolic or functional performance of the beige adipose tissue was maintained and dramatically enhanced over white adipose tissue.

Our study, for the first time, demonstrates key morphological, biological, and functional differences of L-MVF and Db-MVF relating to angiogenesis, WAT, and beige adipose tissue formation, and importantly establishes the first tissue-engineered vascularized beige adipose tissue construct. Given our previous work delineating the importance of adipogenic

induction timing in maximizing and balancing angiogenesis and adipogenesis, in the current study, we analyzed MVF following both direct and indirect (“pre-sprouted”) adipogenic induction to obtain a holistic view of cell source differences.<sup>32</sup> Explicitly, the studies described herein show that MVF from a rodent model of type II diabetes exhibit the capacity for generating vascularized beige adipose tissue with enhanced function. Noting that human metabolism differs than that in rodents, future work shall explore the capacity of human derived MVF in forming vascularized beige adipose tissue.<sup>77,78</sup> Recent preliminary results also suggests that human MVF may also contain beige precursors. In the work depicted, subcutaneous adipose tissue was used for MVF isolation. The ease by which subcutaneous adipose tissue can be isolated using minimally invasive procedures allows for the potential to translate into applications using autologous subcutaneous adipose tissues.<sup>44,45</sup> Future work in understanding metabolic dysfunction should explore whether MVF deriving from diabetic subjects exhibit differences between adipose depots<sup>79</sup> or gender.<sup>80</sup> Moreover, characterization of MVF deriving from other diseased/metabolically altered states should also be characterized, and techniques developed to maximize their adipose and vascular development and function. The influence of tissue mechanical properties and extracellular matrix composition on adipogenic differentiation should also be explored.<sup>46,81,82</sup> Lastly, the impact of transplanting these engineered beige adipose tissues subcutaneously has on whole-body metabolic homeostasis should be investigated.<sup>27,83</sup>

## Materials and Methods

This study was conducted in compliance with the Animal Welfare Act and the Implementing Animal Welfare Regulations in accordance with the principles of the Guide for the Care and Use of Laboratory Animals. All animal procedures were approved by the Institutional Animal Care and Use Committee at the University of Texas at San Antonio.

## Animals

Experiments were carried out using Microvascular fragments (MVF) isolated from obese (FA/FA) or lean (FA/+) male Zucker diabetic fatty (ZDF) rats obtained from Charles River (Wilmington, MA). Rats were acquired at 4 weeks of age and fed Purina 5008 until euthanasia (15–19 weeks of age). Glucose levels (blood from the lateral saphenous vein) were greater than 300 mg/dL in all FA/FA rats used in the study. All animals were housed in a temperature-controlled environment with a 12-hour light–dark cycle and fed *ad libitum*. MVF used in these experiments, for each repetition, were isolated from four different rats, two lean and two diabetic, and pooled to obtain enough cell stock for all studies. All experimental conditions were repeated at least twice.

### **Tissue harvest and microvascular fragment isolation**

MVF were isolated (averaging 40–50  $\mu\text{m}$ ) from both anterior and posterior subcutaneous (SubQ) fat depots similar to that previously described.<sup>84,85</sup> Briefly, the adipose tissue was incubated in collagenase type I (6 mg/mL, Worthington Biochemical Corporation, Lakewood, NJ) at 37°C with agitation for 8–15 minutes, based on visualization of digestion level. The digested material was centrifuged (400 g  $\times$  4 min) resulting in a floating layer of adipocytes and a pellet containing a heterogeneous mixture of cells and MVF. The pellet was resuspended in phosphate-buffered saline (PBS) containing 0.1% bovine serum albumin (Sigma-Aldrich; St. Louis, Mo.) and filtered through 500  $\mu\text{m}$  and 37  $\mu\text{m}$  filters (Carolina Biological Supply, Burlington, NC) to remove large debris and minimize cell contamination, respectively. In detail, the flowthrough from the 500  $\mu\text{m}$  filtration was collected (leaving behind large debris) and then filtered through the 37  $\mu\text{m}$  filter, from which the flowthrough was discarded, and the content entrapped in the filter was dislodged for collection of the MVF. The collected MVF (visualization seen in Supplemental Figure S1) were then counted and centrifuged prior to resuspension in fibrinogen as described below.

### **Scaffold formation and culture conditions**

Fibrin scaffolds were formed by combining 20 mg/mL fibrinogen (Sigma-Aldrich; St. Louis, Mo.) containing 20,000 MVF/mL in DMEM with 10 U/mL thrombin (MilliporeSigma, St. Louis, MO.) in 96-well culture plates, at a 2:5 ratio, with final concentrations being 5.7 mg/mL fibrinogen and 7.1 U/mL thrombin. The hydrogels for gene expression analysis were 100  $\mu\text{L}$  in volume while gels for all other analyzes were 50  $\mu\text{L}$ , except for OCR where 30  $\mu\text{L}$  gels were used.

MVF were cultured under different conditions in order to support angiogenesis, white adipogenic differentiation, or beige adipogenic differentiation (see Figures 1(a) and 4(a) for experimental designs). For angiogenic conditions, MVF were cultured in growth media (GM; Dulbecco's Modified Eagle Medium (DMEM) containing 20% Fetal Bovine Serum, 1% Pen-Strep, and 0.2% MycoZap) for 7, 14, or 21 days. To stimulate adipogenesis, MVF were grown in white adipogenic media (WAM) which consisted of a 4 day treatment with induction media (DMEM/F12 containing 20% Fetal Bovine Serum, 1% Pen-Strep, 0.2% MycoZap, 10  $\mu\text{g}/\text{mL}$  Insulin, 10  $\mu\text{M}$  Forskolin and 1  $\mu\text{M}$  Dexamethasone) followed by maintenance media (DMEM/F12, 20% Fetal Bovine Serum, 1% Pen-Strep, 0.2% MycoZap, and 5  $\mu\text{g}/\text{mL}$  Insulin) for 10 days. Alternatively, MVF were grown in beige adipogenic media (BAM) conditions which consisted of a 4 day treatment with induction media (WAM supplemented with 1  $\mu\text{M}$  Rosiglitazone, and

20 nM T3) followed by maintenance media (WAM supplemented with 10  $\mu\text{M}$  Forskolin, 1  $\mu\text{M}$  Rosiglitazone, and 20 nM T3) for 10 days. Further, to engineer vascularized beige adipose constructs, the MVF fibrin scaffolds were initially grown in GM for 7 days (pre-sprouting) followed by 14 days of either WAM or BAM conditions. For all treatments the medium (100  $\mu\text{L}$  in a 96-well plate) was replaced every other day throughout the study, to avoid pH fluctuations, while cultures were maintained in a humidified incubator at 37°C and 5%  $\text{CO}_2$ .

### **RNA isolation and quantitative RT-PCR**

RNA was isolated from fibrin scaffolds containing MVF ( $n=4$  individual hydrogels/group) and purified using a Qiagen RNeasy Mini Kit (Valencia, CA) according to manufacturer guidelines. Scaffolds were first placed in 1 mL of TRIzol (ThermoFisher, Waltham, MA) and homogenized using a tissue homogenizer (Omni International, Kennesaw, GA), followed by RNA extraction using the Qiagen kit. mRNA concentrations were measured using a Take3 Micro-Volume Plate (BioTek, Winooski, VT), then normalized to 150 ng of mRNA for conversion to cDNA. The isolated RNA was converted to cDNA using the iScript cDNA synthesis kit (BioRad, Hercules, CA). Real-time quantitative polymerase chain reaction (qPCR) was performed using a CFX96 Touch Real-Time PCR Detection System (BioRad, Hercules, CA). All primers (FAS, Adiponectin, PPARG, UCP1, Cidea, FLK1, ANGPT1, and VEGF) used to carry out the analysis were predesigned primers (Sigma-Aldrich; St. Louis, Mo, Supplemental Table S1). Ten  $\mu\text{L}$  of iTaq Universal SYBR Green Supermix (BioRad, Hercules, CA) was used for each reaction. Fold expression levels were calculated using the  $2^{-\Delta\Delta\text{Ct}}$  method, where the GM gels at day 1 were designated as the calibrator group and GAPDH expression was used as the endogenous control.<sup>86</sup>

### **Lipolysis assay**

A lipolysis assay measuring glycerol release was completed using the Lipolysis Colorimetric Assay Kit according to manufacturer's recommendations (BioVision, Milpitas, CA) with a few modifications. Briefly, at the end of the differentiation protocol, gels ( $n=12/\text{group}$ ) were washed two times with provided Lipolysis Wash Buffer, which was then replaced with the Lipolysis Assay Buffer. Ten  $\mu\text{M}$  Isoproterenol (final concentration 100 nM) was added to half the wells to stimulate lipolysis for 3 hr. Following stimulation, 50  $\mu\text{L}$  of media was collected into a 96-well plate and 50  $\mu\text{L}$  reaction mix, provided by the manufacturer, was added and incubated at room temperature for 1 hour, after which absorbance was read at OD 570 nm, with the amount of glycerol released calculated using a standard curve.

### Insulin stimulated glucose uptake assay

Insulin-stimulated glucose analysis was performed according to the manufacturer's instructions (Glucose Uptake-Glo™ Assay, Promega, Madison, WI), with some modifications. Briefly, MVF scaffolds were cultured in DMEM without serum or glucose for 24 hours. Afterward, samples were changed to DMEM ± insulin (1mM) for 2 hours, followed by the addition of 2-Deoxyglucose (0.1 mM) for 1 hour. Finally, a 2-Deoxyglucose-6-phosphate (2DG6P) detection reagent was used to quantify the amount of glucose internalized by the cells. Luminescence was measured after 2 hours with a spectrophotometer (Biotek, Winooski, VT) ( $n=6/\text{group}$ ).

### Immunofluorescence analysis

Hydrogels were fixed in 4% formaldehyde for 2 hours at room temperature, permeabilized using 0.5% Triton-X for 20 minutes, blocked using 10% goat serum for 2 hours, then stained using Rhodamine labeled Griffonia (Bandeiraea) Simplicifolia Lectin I (GS-1; Vector Labs, Burlingame, CA, 1:100), boron-dipyrromethene (BODIPY; ThermoFisher, Waltham, MA, D3922, 1:100), and DAPI (ThermoFisher, Waltham, MA, R37606). The distribution of both vessels and lipid droplets of entire wells ( $n=6/\text{group}$ ) were determined using a Leica TCS SP8 Confocal Microscope (Buffalo Grove, IL) using a rendering of 100  $\mu\text{m}$  thickness/10  $\mu\text{m}$  per section of the entire well. Quantification of "Well Coverage (%)" was performed using the Leica 3D analysis toolkit with Otsu thresholding. Quantification of lipid droplet size (average/well) and number (#/well) was performed using ImageJ (U. S. National Institutes of Health, Bethesda, MD) followed by a custom MATLAB (MathWorks, Natick, MA) script (Supplementary Text).

### ROS assay—hydrogen peroxide assay

The ROS-Glo H<sub>2</sub>O<sub>2</sub> Assay uses a modified luciferin substrate, based on boronate oxidation, which reacts directly with hydrogen peroxide (H<sub>2</sub>O<sub>2</sub>) to generate a luciferin precursor. Upon addition of detection reagent, the precursor is converted to luciferin and Ultra-Glo Recombinant Luciferase included in the detection reagent produces a light signal proportional to the level of H<sub>2</sub>O<sub>2</sub> in the sample. A mixture of the H<sub>2</sub>O<sub>2</sub> substrate and H<sub>2</sub>O<sub>2</sub> dilution buffer (150  $\mu\text{L}$ ) was added to each well containing the scaffolds. Six hours later, 50  $\mu\text{L}$  of the media was mixed with 50  $\mu\text{L}$  of ROS-GLO Detection Solution in a separate plate and incubated at room temperature for 20 minutes. Luminescence was read using a Take3 Micro-Volume Plate (BioTek, Winooski, VT).

### OCR analysis

A mitochondrial stress test was performed to analyze the cellular metabolic activity of the differentiated 3D culture models ( $n=10/\text{group}$ ) using a Seahorse XF96 Flux

Analyzer (Seahorse Bioscience). The XF Analyzer measures the oxygen consumption rate (OCR) of live cells in real-time. The sequential application of drugs that inhibit different electron transport chain enzymes (ETC) is utilized to determine metabolic parameters such as basal and maximal cellular respiration, proton leak, and spare capacity.<sup>87</sup>

At the start of the assay, an initial OCR reading was performed. Oligomycin was added to the culture wells to inhibit ATP synthase, reducing the contribution of ATP production and revealing proton leak in the ETC (after correcting for nonmitochondrial oxygen consumption). Second, the ionophore carbonyl cyanide-p-trifluoromethoxyphenylhydrazone (FCCP) was applied to induce maximum respiration. Finally, rotenone and antimycin A were used to inhibit the ETC enzymes upstream of oxygen consumption, thus eliminating all mitochondrial oxygen expenditure. The final OCR represents the background nonmitochondrial oxygen consumption of the cells. Subtracting the final OCR after rotenone/antimycin A treatment from initial OCR before oligomycin treatment gives the basal mitochondrial metabolism or the mitochondrial OCR at resting state.<sup>88</sup>

For OCR measurement, fibrin gels (30  $\mu\text{L}$ ), as described previously, were seeded into XF96 V3 PS Tissue Culture Microplates and cultured for either 14 or 21 days (based on groups as described previously), cells were then placed in a 37°C incubator without CO<sub>2</sub> for 45 minutes before the assay. After basal measurements, oligomycin (1 mM), FCCP (250 nM), and rotenone/antimycin A (2 mM/2 mM) were injected sequentially to characterize the mitochondrial function of the cells. Six measurements were taken before and following the application of each drug solution. Oligomycin, FCCP, and rotenone/antimycin A were injected into the medium at 42, 84, and 126 minutes, respectively.

### Statistical analysis

GraphPad Prism Software 7 (GraphPad Software, Inc., La Jolla, CA) was used to run one, or two-way analysis of variance (ANOVA) tests with Holm-Sidak's multiple comparison analyzes to determine differences between groups. Statistical significance was defined as  $p < 0.05$ . All results are presented as mean ± standard error of the mean (SEM).

### Author Contributions

Conceptualization: FMA, KS, CRR, EMB

Methodology: FMA, KS, JZ, EIG

Investigation: FMA, KS, JZ, EIG

Visualization: FMA, KS

Supervision: JXJ, CRR, EMB

Writing—original draft: FMA, KS

Writing—review & editing: FMA, KS, JZ, EIG, JXJ, CRR, EMB

### Declaration of Conflicting Interests

The author(s) declared no potential conflicts of interest with respect to the research, authorship, and/or publication of this article.

## Funding

The author(s) disclosed receipt of the following financial support for the research, authorship, and/or publication of this article: National Institutes of Health grant SC1DK122578 (CRR) National Institutes of Health grant 5RO1EB020604 (EMB) National Institutes of Health grant GM060655 (FMA) National Institutes of Health grant CA148724 (FMA) Veterans Administration grant 5 I01 BX000418-06 (EMB) University of Texas System Science and Technology Acquisition and Retention Program University of Texas Department of Biomedical Engineering and Chemical Engineering

## ORCID iD

Eric M. Brey  <https://orcid.org/0000-0001-8766-7390>

## Data and materials availability

All data are available in the main text or the supplementary materials.

## Supplemental material

Supplemental material for this article is available online.

## References

- Saklayen MG. The global epidemic of the metabolic syndrome. *Curr Hypertens Rep* 2018; 20: 12–12.
- Poirier P, Giles TD, Bray GA, et al. Obesity and cardiovascular disease: pathophysiology, evaluation, and effect of weight loss: an update of the 1997 American Heart Association Scientific Statement on Obesity and heart disease from the Obesity Committee of the Council on Nutrition, physical activity, and metabolism. *Circulation* 2006; 113: 898–918.
- Wolin KY, Carson K and Colditz GA. Obesity and cancer. *Oncologist* 2010; 15: 556–565.
- Eckel RH, Kahn SE, Ferrannini E, et al. Obesity and type 2 diabetes: what can be unified and what needs to be individualized? *J Clin Endocrinol Metab* 2011; 96: 1654–1663.
- Kim DD and Basu A. Estimating the medical care costs of obesity in the United States: systematic review, meta-analysis, and empirical analysis. *Value Health* 2016; 19: 602–613.
- Choe SS, Huh JY, Hwang IJ, et al. Adipose tissue remodeling: its role in energy metabolism and metabolic disorders. *Front Endocrinol* 2016; 7: 30.
- Barquissau V, Beuzelin D, Pisani DF, et al. White-to-brite conversion in human adipocytes promotes metabolic reprogramming towards fatty acid anabolic and catabolic pathways. *Mol Metab* 2016; 5: 352–365.
- Rosell M, Kafrou M, Frontini A, et al. Brown and white adipose tissues: intrinsic differences in gene expression and response to cold exposure in mice. *Am J Physiol Endocrinol Metab* 2014; 306: E945–E964.
- Yang JP, Anderson AE, McCartney A, et al. Metabolically active three-dimensional brown adipose tissue engineered from white adipose-derived Stem Cells. *Tissue Eng Part A* 2017; 23: 253–262.
- Kurylowicz A and Puzianowska-Kuznicka M. Induction of Adipose Tissue Browning as a strategy to combat obesity. *Int J Mol Sci* 2020; 21: 6241.
- Srivastava S and Veech RL. Brown and Brite: the Fat Soldiers in the anti-obesity fight. *Front Physiol* 2019; 10: 38.
- Kaisanlahti A and Glumoff T. Browning of white fat: agents and implications for beige adipose tissue to type 2 diabetes. *J Physiol Biochem* 2019; 75: 1–10.
- Mulya A and Kirwan JP. Brown and beige adipose tissue: Therapy for obesity and its comorbidities? *Endocrinol Metab Clin North Am* 2016; 45: 605–621.
- Lizcano F and Vargas D. Biology of beige adipocyte and possible therapy for type 2 diabetes and obesity. *Int J Endocrinol* 2016; 2016: 9542061.
- Cohen P and Spiegelman BM. Brown and beige fat: molecular parts of a thermogenic machine. *Diabetes* 2015; 64: 2346–2351.
- Wu J, Cohen P and Spiegelman BM. Adaptive thermogenesis in adipocytes: is beige the new brown? *Genes Dev* 2013; 27: 234–250.
- Wang C-H, Lundh M, Fu A, et al. CRISPR-engineered human brown-like adipocytes prevent diet-induced obesity and ameliorate metabolic syndrome in mice. *Sci Transl Med* 2020; 12: eaaz8664.
- Cypess AM, Lehman S, Williams G, et al. Identification and importance of brown adipose tissue in adult humans. *New Engl J Med* 2009; 360: 1509–1517.
- Loyd C and Obici S. Brown fat fuel use and regulation of energy homeostasis. *Curr Opin Clin Nutr Metab Care* 2014; 17: 368–372.
- Wankhade UD, Shen M, Yadav H, et al. Novel Browning Agents, mechanisms, and therapeutic potentials of brown adipose tissue. *Biomed Res Int* 2016; 2016: 2365609.
- Tharp KM and Stahl A. Bioengineering Beige Adipose Tissue Therapeutics. *Front Endocrinol* 2015; 6: 164.
- Vaicik MK, Morse M, Blagajcevic A, et al. Hydrogel-based engineering of Beige Adipose Tissue. *J Mater Chem B* 2015; 3: 7903–7911.
- McCarthy M, Brown T, Alarcon A, et al. Fat-On-A-Chip models for research and discovery in obesity and its metabolic comorbidities. *Tissue Eng Part B Rev* 2020; 26: 586–595.
- Murphy CS, Liaw L and Reagan MR. In vitro tissue-engineered adipose constructs for modeling disease. *BMC Biomed Eng* 2019; 1, 27. DOI: 10.1186/s42490-019-0027-7
- Unser AM, Tian Y and Xie Y. Opportunities and challenges in three-dimensional brown adipogenesis of stem cells. *Biotechnol Adv* 2015; 33: 962–979.
- Klingelhutz AJ, Gourronc FA, Chaly A, et al. Scaffold-free generation of uniform adipose spheroids for metabolism research and drug discovery. *Sci Rep* 2018; 8: 523.
- Tharp KM, Jha AK, Kraiczky J, et al. Matrix-assisted transplantation of functional beige adipose tissue. *Diabetes* 2015; 64: 3713–3724.
- Harms MJ, Li Q, Lee S, et al. Mature human white adipocytes cultured under membranes maintain identity, function, and can transdifferentiate into brown-like adipocytes. *Cell Rep* 2019; 27: 213–225.e5.
- Hepler C, Vishvanath L and Gupta RK. Sorting out adipocyte precursors and their role in physiology and disease. *Genes Dev* 2017; 31: 127–140.

30. Tran KV, Gealekman O, Frontini A, et al. The vascular endothelium of the adipose tissue gives rise to both white and brown fat cells. *Cell Metab* 2012; 15: 222–229.
31. McDaniel JS, Pilia M, Ward CL, et al. Characterization and multilineage potential of cells derived from isolated microvascular fragments. *J Surg Res* 2014; 192: 214–222.
32. Acosta FM, Stojkova K, Brey EM, et al. A straightforward approach to engineer vascularized adipose tissue using microvascular fragments. *Tissue Eng Part A* 2020; 26: 905–914.
33. Reynolds Th 4TH, Banerjee S, Sharma VM, et al. Effects of a high fat diet and voluntary wheel running exercise on cidea and cidec expression in liver and adipose tissue of Mice. *PLoS One* 2015; 10: e0130259.
34. Corvera S and Gealekman O. Adipose tissue angiogenesis: impact on obesity and type-2 diabetes. *Biochimica et Biophysica Acta (BBA) - Molecular Basis of Disease* 2014; 1842: 463–472.
35. Gealekman O, Guseva N, Gurav K, et al. Effect of rosiglitazone on capillary density and angiogenesis in adipose tissue of normoglycaemic humans in a randomised controlled trial. *Diabetologia* 2012; 55: 2794–2799.
36. Gealekman O, Guseva N, Hartigan C, et al. Depot-specific differences and insufficient subcutaneous adipose tissue angiogenesis in human obesity. *Circulation* 2011; 123: 186–194.
37. Laschke MW, Später T and Menger MD. Microvascular fragments: more than just natural vascularization units. *Trends Biotechnol* 2021; 39: 24–33.
38. Dlasková A, Clarke KJ and Porter RK. The role of UCP 1 in production of reactive oxygen species by mitochondria isolated from brown adipose tissue. *Biochimica et Biophysica Acta (BBA) - Bioenergetics* 2010; 1797: 1470–1476.
39. Samuelson I and Vidal-Puig A. Studying brown adipose tissue in a human in vitro context. *Front Endocrinol* 2020; 11: 629.
40. Stanford KI, Middelbeek RJ, Townsend KL, et al. Brown adipose tissue regulates glucose homeostasis and insulin sensitivity. *J Clin Investig* 2013; 123: 215–223.
41. Liu X, Wang S, You Y, et al. Brown adipose tissue transplantation reverses obesity in Ob/Ob Mice. *Endocrinology* 2015; 156: 2461–2469.
42. Sato N, Sawasaki Y, Senoo A, et al. Development of capillary networks from rat microvascular fragments in vitro: the role of myofibroblastic cells. *Microvasc Res* 1987; 33: 194–210.
43. Laschke MW and Menger MD. The simpler, the better: tissue vascularization using the body's own resources. *Trends Biotechnol* 2022; 40: 281–290.
44. Strobel HA, Gerton T and Hoying JB. Vascularized adipocyte organoid model using isolated human microvessel fragments. *Biofabrication* 2021; 13: 035022.
45. Xu X, Liang C, Gao X, et al. Adipose tissue-derived microvascular fragments as vascularization units for dental pulp regeneration. *J Endod* 2021; 47: 1092–1100.
46. Acosta FM, Howland KK, Stojkova K, et al. Adipogenic differentiation alters properties of vascularized tissue-engineered skeletal muscle. *Tissue Eng Part A* 2022; 28: 54–68.
47. Wang QA, Scherer PE and Gupta RK. Improved methodologies for the study of adipose biology: insights gained and opportunities ahead. *J Lipid Res* 2014; 55: 605–624.
48. Kim SH and Plutzky J. Brown fat and Browning for the treatment of obesity and related metabolic disorders. *Diabetes Metab J* 2016; 40: 12–21.
49. Coolbaugh CL, Damon BM, Bush EC, et al. Cold exposure induces dynamic, heterogeneous alterations in human brown adipose tissue lipid content. *Sci Rep* 2019; 9: 13600.
50. Cui Y, Xu X, Bi H, et al. Expression modification of uncoupling proteins and MnSOD in retinal endothelial cells and pericytes induced by high glucose: the role of reactive oxygen species in diabetic retinopathy. *Exp Eye Res* 2006; 83: 807–816.
51. Mourad O, Nkenkor B and Nunes SS. Chapter 22 – Compounding effects of diabetes in vessel formation in microvessel fragment-based engineered constructs. *The Science, Etiology and Mechanobiology of Diabetes and its Complications*: Academic Press, 2021; pp. 375–387.
52. Aghazadeh Y, Poon F, Sarangi F, et al. Microvessels support engraftment and functionality of human islets and hESC-derived pancreatic progenitors in diabetes models. *Cell Stem Cell* 2021; 28: 1936–1949.e8.
53. Hiscox AM, Stone AL, Limesand S, et al. An islet-stabilizing implant constructed using a preformed vasculature. *Tissue Eng Part A* 2008; 14: 433–440.
54. Salamone M, Rigogliuso S, Nicosia A, et al. 3D collagen hydrogel promotes in vitro Langerhans islets vascularization through ad-MVFs angiogenic activity. *Biomedicines* 2021; 9: 739.
55. Altalhi W, Hatkar R, Hoying JB, et al. Correction to: Type I diabetes delays perfusion and engraftment of 3D constructs by impinging on angiogenesis; which can be rescued by hepatocyte growth factor supplementation. *Cell Mol Bioeng* 2019; 12: 541–542.
56. Altalhi W, Sun X, Sivak JM, et al. Diabetes impairs arterio-venous specification in engineered vascular tissues in a perivascular cell recruitment-dependent manner. *Biomaterials* 2017; 119: 23–32.
57. Laschke MW, Grässer C, Kleer S, et al. Adipose tissue-derived microvascular fragments from aged donors exhibit an impaired vascularisation capacity. *Eur Cell Mater* 2014; 28: 287–298.
58. Huttala O, Palmroth M, Hemminki P, et al. Development of versatile human *In Vitro* Vascularized adipose tissue model with serum-free angiogenesis and natural adipogenesis induction. *Basic Clin Pharmacol Toxicol* 2018; 123(Suppl 5): 62–71.
59. Christiaens V and Lijnen HR. Angiogenesis and development of adipose tissue. *Mol Cell Endocrinol* 2010; 318: 2–9.
60. Weinzierl A, Harder Y, Schmauss D, et al. Improved vascularization and survival of white compared to brown adipose tissue grafts in the dorsal skinfold chamber. *Biomedicines* 2021; 10: 23.
61. Herold J and Kalucka J. Angiogenesis in adipose tissue: the interplay between adipose and Endothelial Cells. *Front Physiol* 2020; 11: 624903.
62. Laschke MW, Kontaxi E, Scheuer C, et al. Insulin-like growth factor 1 stimulates the angiogenic activity of adipose tissue-derived microvascular fragments. *J Tissue Eng* 2019; 10: 2041731419879837.
63. Laschke MW, Seifert MS, Scheuer C, et al. High glucose exposure promotes proliferation and in vivo network formation of adipose-tissue-derived microvascular fragments. *Eur Cell Mater* 2019; 38: 188–200.



64. Ye J, Gao Z, Yin J, et al. Hypoxia is a potential risk factor for chronic inflammation and adiponectin reduction in adipose tissue of *ob/ob* and dietary obese mice. *Am J Physiol Endocrinol Metab* 2007; 293: E1118–E1128.
65. Freiman A, Shandalov Y, Rozenfeld D, et al. Adipose-derived endothelial and mesenchymal stem cells enhance vascular network formation on three-dimensional constructs in vitro. *Stem Cell Res Ther* 2016; 7: 5.
66. Später T, Menger MM, Nickels RM, et al. Macrophages promote network formation and maturation of transplanted adipose tissue-derived microvascular fragments. *J Tissue Eng* 2020; 11: 2041731420911816.
67. Später T, Körbel C, Frueh FS, et al. Seeding density is a crucial determinant for the in vivo vascularisation capacity of adipose tissue-derived microvascular fragments. *Eur Cell Mater* 2017; 34: 55–69.
68. Edgar LT, Underwood CJ, Guilkey JE, et al. Extracellular matrix density regulates the rate of neovessel growth and branching in sprouting angiogenesis. *PLoS One* 2014; 9: e85178.
69. Chiou G, Jui E, Rhea AC, et al. Scaffold architecture and matrix strain modulate mesenchymal cell and microvascular growth and development in a time dependent manner. *Cell Mol Bioeng* 2020; 13: 507–526.
70. Yang F, Cohen RN and Brey EM. Optimization of Co-culture conditions for a human vascularized adipose tissue model. *Bioengineering* 2020; 7: 114.
71. Volpe CMO, Villar-Delfino PH, Dos Anjos PMF, et al. Cellular death, reactive oxygen species (ROS) and diabetic complications. *Cell Death Dis* 2018; 9: 119–119.
72. Zhou Y, Li H and Xia N. The interplay between adipose tissue and vasculature: role of oxidative stress in Obesity. *Front Cardiovasc Med* 2021; 8: 650214.
73. Patti ME and Corvera S. The role of mitochondria in the pathogenesis of type 2 diabetes. *Endocr Rev* 2010; 31: 364–395.
74. Prasun P. Role of mitochondria in pathogenesis of type 2 diabetes mellitus. *J Diabetes Metab Disord* 2020; 19: 2017–2022.
75. Alcalá M, Calderon-Dominguez M, Bustos E, et al. Increased inflammation, oxidative stress and mitochondrial respiration in brown adipose tissue from obese mice. *Sci Rep* 2017; 7: 16082.
76. Shabalina IG, Vrbacký M, Pecinová A, et al. ROS production in brown adipose tissue mitochondria: the question of UCP1-dependence. *Biochimica et Biophysica Acta (BBA) - Bioenergetics* 2014; 1837: 2017–2030.
77. Fuller KNZ and Thyfault JP. Barriers in translating preclinical rodent exercise metabolism findings to human health. *J Appl Physiol* 2021; 130: 182–192.
78. Cannon B, de Jong JMA, Fischer AW, et al. Human brown adipose tissue: Classical brown rather than brite/beige? *Exp Physiol* 2020; 105: 1191–1200.
79. Später T, Marschall JE, Brücker LK, et al. Vascularization of microvascular fragment isolates from visceral and subcutaneous adipose tissue of Mice. *Tissue Eng Regen Med* 2022; 19: 161–175.
80. Später T, Marschall JE, Brücker LK, et al. Adipose tissue-derived microvascular fragments from male and female fat donors exhibit a comparable vascularization capacity. *Front Bioeng Biotechnol* 2021; 9: 777687.
81. Gonzalez Porras MA, Stojkova K, Vaicik MK, et al. Integrins and extracellular matrix proteins modulate adipocyte thermogenic capacity. *Sci Rep* 2021; 11: 5442.
82. Kuss M, Kim J, Qi D, et al. Effects of tunable, 3D-bioprinted hydrogels on human brown adipocyte behavior and metabolic function. *Acta Biomater* 2018; 71: 486–495.
83. Dani V, Yao X and Dani C. Transplantation of fat tissues and iPSC-derived energy expenditure adipocytes to counteract obesity-driven metabolic disorders: Current strategies and future perspectives. *Rev Endocr Metab Disord* 2022; 23: 103–110.
84. Stone R 2nd and Rathbone CR. Microvascular fragment transplantation improves rat dorsal skin flap survival. *Plast Reconstr Surg Glob Open* 2016; 4: e1140. 2017.
85. Frueh FS, Später T, Scheuer C, et al. Isolation of murine adipose tissue-derived microvascular fragments as vascularization units for tissue engineering. *Journal of visualized experiments: JoVE* 2017; 122: 55721. DOI: 10.3791/55721
86. Livak KJ and Schmittgen TD. Analysis of relative gene expression data using real-time quantitative PCR and the 2- $\Delta\Delta$ CT method. *Methods* 2001; 25: 402–408.
87. Ferrick DA, Neilson A and Beeson C. Advances in measuring cellular bioenergetics using extracellular flux. *Drug Discov Today* 2008; 13: 268–274.
88. Dranka BP, Benavides GA, Diers AR, et al. Assessing bioenergetic function in response to oxidative stress by metabolic profiling. *Free Radic Biol Med* 2011; 51: 1621–1635.